Core@shell structured ceria@mesoporous silica nanoantibiotics restrain bacterial growth in vitro and in vivo

Karaman, Didem Şen; Kietz, Christa; Govardhanam, Prakirth; Slita, Anna; Manea, Alexandra; Pamukçu, Ayşenur; Meinander, Annika; Rosenholm, Jessica M.

Published in:
Materials Science and Engineering: C

DOI:
10.1016/j.msec.2021.112607

Published: 01/02/2022

Document Version
Final published version

Biomaterials Advances 133 (2022) 112607

Contents lists available at ScienceDirect

Biomaterials Advances

journal homepage: www.elsevier.com/locate/bioadv

Core@shell structured ceria@mesoporous silica nanoantibiotics restrain bacterial growth *in vitro and in vivo*

Didem Şen Karaman [a,*], Christa Kietz [b,1], Prakirth Govardhanam [c,1], Anna Slita [c], Alexandra Manea [c], Ayşenur Pamukçu [a], Annika Meinander [b,*], Jessica M. Rosenholm [c]

[a] Department of Biomedical Engineering, Faculty of Engineering and Architecture, İzmir Katip Çelebi University, İzmir, Turkey
[b] Cell Biology, Faculty of Science and Engineering, Åbo Akademi University, Finland
[c] Pharmaceutical Sciences Laboratory, Faculty of Science and Engineering, Åbo Akademi University, Finland

ARTICLE INFO

Keywords:
Cerium oxide
Core@shell
Capsaicin
Chitosan
Mesoporous silica
Nanoantibiotic
Escherichia coli
Drosophila melanogaster

ABSTRACT

Due to its modular and flexible design options, mesoporous silica provides ample opportunities when developing new strategies for combinatory antibacterial treatments. In this study, antibacterial ceria (CeO_2) nanoparticles (NP) were used as core material, and were further coated with a mesoporous silica shell ($mSiO_2$) to obtain a core@shell structured nanocomposite (CeO_2@$mSiO_2$). The porous silica shell was utilized as drug reservoir, whereby CeO_2@$mSiO_2$ was loaded with the antimicrobial agent capsaicin (CeO_2@$mSiO_2$/Cap). CeO_2@$mSiO_2$/Cap was further surface-coated with the natural antimicrobial polymer chitosan by employing physical adsorption. The obtained nanocomposite, CeO_2@$mSiO_2$/Cap@Chit, denoted NAB, which stands for "*nanoantibiotic*", provided a combinatory antibacterial mode of action. The antibacterial effect of NAB on the Gram-negative bacteria *Escherichia coli (E.coli)* was proven to be significant *in vitro*. In addition, *in vivo* evaluations revealed NAB to inhibit the bacterial growth in the intestine of bacteria-fed *Drosophila melanogaster* larvae, and decreased the required dose of capsaicin needed to eliminate bacteria. As our constructed CeO_2@$mSiO_2$ did not show toxicity to mammalian cells, it holds promise for the development of next-generation nanoantibiotics of non-toxic nature with flexible design options.

1. Introduction

The unique properties of nanomaterials compared to their bulk counterparts render them favored for antibacterial therapies. Nanostructured materials can be used to convey antimicrobials, assist in the delivery of drugs, or as antimicrobial agents themselves [1,2]. Most studies have focused on inorganic nanoparticles (NP) containing silver, gold, copper, zinc, titanium oxide, and cerium oxide as antibacterial agents [3]. Metal-based nanoparticles have non-specific antibacterial mechanisms, which may circumvent the development of antibiotic resistance mechanisms (AMR), broaden the spectrum of antibacterial activity and inhibit biofilm formation [1–4]. In recent years, there have been numerous studies on the use of cerium and cerium oxide-based nanomaterials in medical sciences [5,6]. They are found to be used as anticancer, antioxidant, antibacterial, antibiofilm and anti-inflammatory drugs, and for bioscaffold design for tissue engineering [7]. However, aggregation of pristine CeO_2 NP, like other metal-oxide nanoparticles could impede their widespread usage. Thus, standardization of the dispersing protocol or development of different design strategies is necessary to overcome this obstacle [8]. Employing surfactants as dispersing agents, storage in a dryer, and sonication of the nanoparticles are among the used approaches [9,10]. Another approach for preventing the aggregation of metal/metal oxide nanoparticles is coating the core with a layer of another organic or/and inorganic material (shell) [11]. In these so-called core@shell designs, mesoporous silica ($mSiO_2$) offers superior advantages as a coating material. The main advantages of silica as shell material lies in its colloidal stability, especially in aqueous media; flexible design options, chemical inertness, controlled porosity, high processability and optical transparency [12]. The chemical inertness of silica can shield the core from degradation and provide multifunctionality. Importantly, the incorporation of several antibacterial constructs with different properties into one system allows for combinatorial antibacterial action and increased possibilities for bacterial targeting [2].

Adding to the prospects of combinatorial therapy, we designed nanocomposites consisting of CeO_2 NP with inherent antibacterial properties as core material, and a mesoporous silicon dioxide ($mSiO_2$) shell acting as a reservoir for antibacterial compounds, in the present case capsaicin [8,13,14]. Finally, in order to improve the antimicrobial properties of the nanocomposite, the $mSiO_2$ shell was surface-coated by absorption with the antibacterial polymer chitosan. Chitosan provides improved adhesion to bacterial surfaces and serves as a chelating agent for ions released from the CeO_2 core [15–18] (Scheme 1). We hypothesized that core@shell

* Corresponding authors.
E-mail addresses: didem.sen.karaman@ikcu.edu.tr (D. Şen Karaman), Annika.Meinander@abo.fi (A. Meinander).
[1] Equal contribution.

http://dx.doi.org/10.1016/j.msec.2021.112607
Received 23 August 2021; Received in revised form 2 December 2021; Accepted 8 December 2021
Available online 14 December 2021

structured nanocomposites would improve the overall antibacterial effect by providing a multifaceted action disturbing growth rate and destructing the bacterial cell morphology. The capsaicin-loaded and chitosan-coated CeO_2@$mSiO_2$ (NAB) and its constructs were evaluated for effects against Gram-negative *Escherichia coli* (*E. coli*) *in vitro* and *in vivo*. *E. coli* was chosen as test bacteria as it is available as transformable competent strains. These strains can be detected specifically and distinguished from the commensal microflora resident in the intestine of the model organism *Drosophila melanogaster*. The NAB design was shown to increase the antibacterial potential of its constructs and have potential of operability *in vivo*.

2. Materials and methods

2.1. Synthesis of CeO_2 NP and core@shell structured nanocomposites (CeO_2@$mSiO_2$)

The core unit of NAB, CeO_2 NP was synthesized by two-stage non-isothermal precipitation. 0.26 M precursor solution was prepared by dissolving cerium (III) nitrate hexahydrate (99% trace metals basis) in deionized water and stirred at 70 °C under reflux. The pH was as increased and maintained at 8.8 with the addition of 3 M ammonium hydroxide solution. The solution was incubated at 65 °C for 20 h for the aging of cerium hydroxide ($Ce(OH)_3$) precipitate [19]. At the so-called aging stage, the precipitates were further dehydrated and underwent dissolution–recrystallization under ambient atmosphere. After incubation, the solution was centrifuged at 8000 rpm for 10 min at 22 °C. Centrifugation and washing was repeated three times with absolute ethanol. The final product was kept as suspension and stored at +4 °C.

A shell of mesoporous silica ($mSiO_2$) around the CeO_2 core was prepared by employing chemical wet technique of the sol-gel process. Briefly, CeO_2 NP was dispersed at 1 mg/ml concentration and ultra-sonicated. A reaction solution, consisting of 4.3 ml deionized water, 2.9 ml absolute ethanol, and 40 μl of 32% ammonia was prepared and the CeO_2 NP suspension was added dropwise to the reaction solution under sonication. The mixture was sonicated for 30 min. A surfactant solution was prepared using 40 mg hexadecyltrimethylammonium bromide (CTAB) (≥99%), 660 μl milli-Q water, and 300 μl absolute ethanol. The surfactant solution was added dropwise to the reaction mixture under sonication. Later, 80 μl of tetraethyl orthosilicate (≥99%, TEOS), used as the precursor of silica was added dropwise to the mixture. The reaction mixture was left for stirring at room temperature for 18 h [20]. The product was collected and centrifuged at 12,000 rpm (~17,200 rcf) to remove unreacted chemicals. The sonication, washing and centrifugation were performed three times in sequence with 20% (w/v) ammonium nitrate ethanol solution to remove the surfactant template of $mSiO_2$. The product namely CeO_2@$mSiO_2$, was stored in acetone dispersion at +4 °C.

2.2. Loading of capsaicin and chitosan coating of core@shell nanocomposites

To contribute to the combinatory antibacterial activity of the nanocomposite, the mesoporous shell architecture of CeO_2@$mSiO_2$ was employed as reservoir for capsaicin (Capsaicin-natural (65% capsaicin, 35% dihydrocapsaicin)). Solvent immersion was perfomed to accomplish the

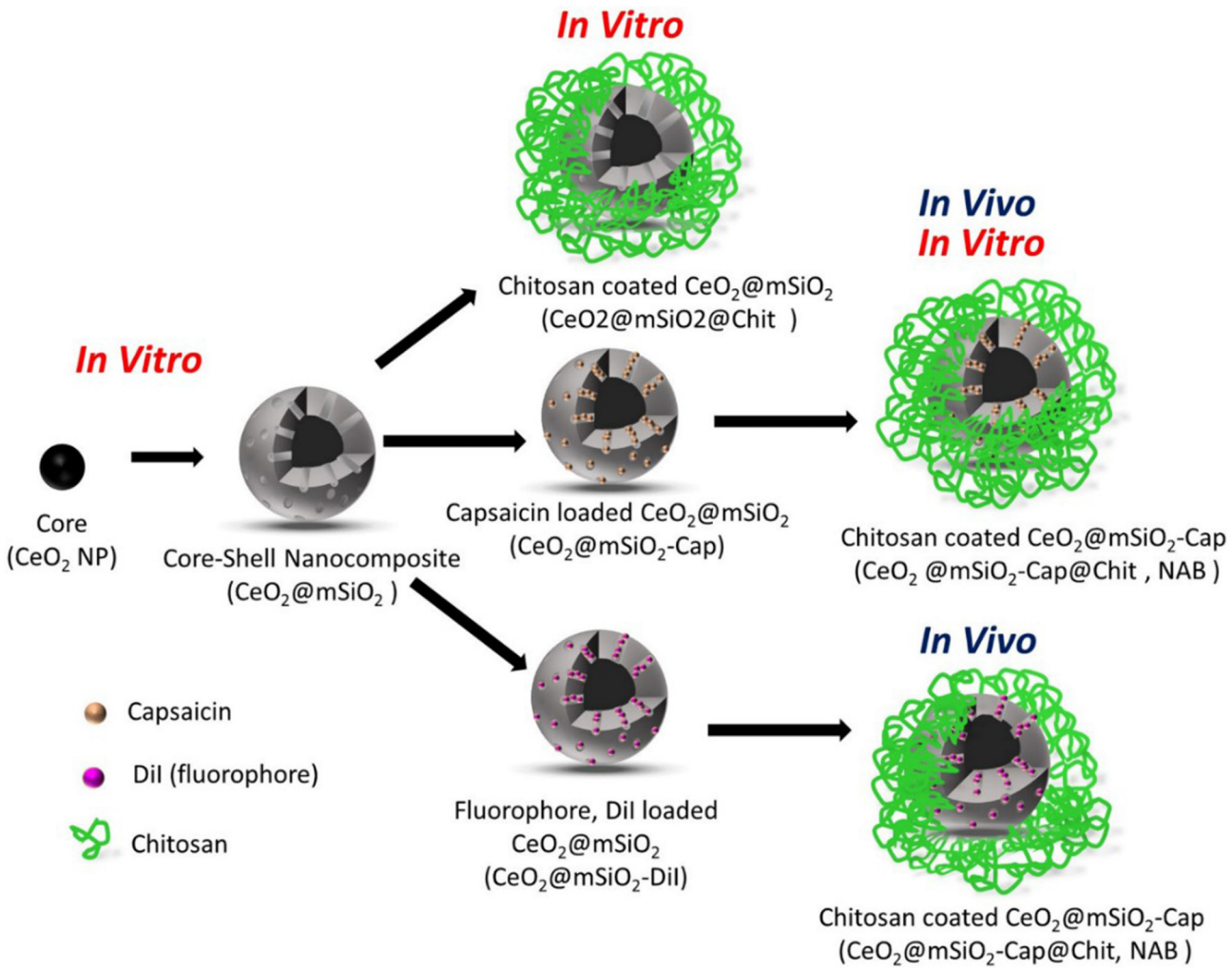

Scheme 1. Schematic representation of the different constructs of NAB developed in this study.

capsaicin loading into mesoporous shell of the nanocomposite design [21]. Briefly, 20 mg of CeO_2@$mSiO_2$ was soaked into different concentrations of 10 ml capsaicin cyclohexane solution and kept on rotating wheel overnight. Afterwards, capsaicin loaded CeO_2@$mSiO_2$ (CeO_2@$mSiO_2$-Cap) was collected by centrifugation and vacuum dried. The adsorption isotherm was obtained by ethanol elution as a function of equilibrium concentration as described the in Supplementary Material and presented in Fig. S1. The highest loading degree could be obtained by treating the CeO_2@$mSiO_2$ with starting capsaicin loading degree of 50 w/w% with respect to the CeO_2@$mSiO_2$ nanocomposites and employed for further preparations.

The surface coating of CeO_2@$mSiO_2$-Cap was carried out by physical adsorption of chitosan polymer (Low molecular weight (186 KDa) 75–85% deacetylated) in acetate buffer (pH 4.7–5.0, 10 mM) solution [22]. The adsorption was performed by dispersing CeO_2@$mSiO_2$-Cap in a sonication bath for 15 min and mixing with chitosan solution (50 w/w% respect to mass of CeO_2@$mSiO_2$-Cap). Subsequently, the mixture was allowed to stir for 4 h. The final product, CeO_2@$mSiO_2$-Cap@Chit, or shortly termed as nanoantibiotics (NAB), was centrifuged and the precipitate was taken for lyophilization. The supernatant was taken for spectrophotometric analysis to investigate the leached out capsaicin during the chitosan coating process.

2.3. Characterization of core@shell structured nanocomposite

2.3.1. Hydrodynamic size (DLS) and net surface charge (ζ-potential) measurements

Dynamic light scattering and electrophoresis techniques were employed to analyze hydrodynamic size and ζ-potential values of CeO_2, CeO_2@$mSiO_2$, CeO_2@$mSiO_2$-Cap and CeO_2@$mSiO_2$-Cap@Chit dispersions prepared in acetate buffer (pH 5, 10 mM) by using a sonication bath. The measurements were performed using the Zetasizer Nano ZS instrument.

2.3.2. Transmission electron microscopy imaging of NAB

TEM imaging was performed to analyze the morphology of synthesized CeO_2 NP, CeO_2@$mSiO_2$, and the preserved composition of NAB. TEM specimens were prepared by drop casting of the nanocomposite suspensions on TEM grids and examined using JEOL JEM-1400 Plus, operated at 80 kV. TEM micrograms of nanocomposites were employed to estimate the particle size distribution of CeO_2@$mSiO_2$ by analyzing the number of 1113 different images of nanocomposite structures. These images have been analyzed using the 'Analyze Particles' method from ImageJ2 [23]. Particle size distribution analysis from TEM micrographs was performed through the cumulative frequency distribution of particles [24].

2.3.3. Cerium element release from CeO_2@$mSiO_2$ and CeO_2@$mSiO_2$@Chit

The cerium element release investigations were performed by dispersing weighed CeO_2@$mSiO_2$ and CeO_2@$mSiO_2$@Chit samples in the aqueous solution at a concentration of 100 μg/ml, and incubating in Spectra/PorsFloat-A-LyzersG1, Ready-to-Use laboratory dialysis devices for 48 h. Measurements were carried out in the standard mode of a quadruple ICP-MS instrument. Samples for each time point were measured 3 times, and the average value of the measurements was used to plot the cerium release profiles. To determine the total amount of cerium element in CeO_2 NP and CeO_2@$mSiO_2$, nanoparticles were digested by ultrasonic bath and microwave-assisted mineralization with diluted HNO_3 [25]. The obtained numerical values were used to estimate the relative cerium element release percentage with respect to the starting concentration of the cerium element in time.

2.3.4. Release of capsaicin from CeO_2@$mSiO_2$-Cap and CeO_2@$mSiO_2$-Cap@Chit

Capsaicin release profiles and the pH responsiveness of the chitosan coating on the NAB were investigated by following release of capsaicin from CeO_2@$mSiO_2$_Cap@Chit and CeO_2@$mSiO_2$-Cap at two different pH 5 in acetate buffer solution and pH 7.2 in HEPES buffer solution at 36 °C for 24 h. The dispersion of CeO_2@$mSiO_2$_Cap and CeO_2@$mSiO_2$-Cap@Chit samples at a concentration of 1 mg/ml were incubated in a shaking incubator at 200 rpm at 37 °C. The incubation was terminated at 1 h, 2 h, 4 h, 8 h, 10 h, and 24 h, and the released capsaicin was measured by UV-VIS spectrophotometer at 280 nm after removing particles by centrifugation. Samples of each time point were measured 3 times and the average value of the measurements was plotted.

2.4. In vitro cytocompatibility of NAB and its constructs

The human colorectal adenoma cell line, Caco-2, was employed as the model cell line of intestinal barrier to evaluate cytocompatibility of NAB and its constructs [26]. The cells were grown in complete Dulbecco's Modified Eagle's Medium (Lonza BioWhittaker, Basel, Switzerland) (with 25 mM HEPES buffer and 4.5 g/l Glucose) with an addition of 10% heat-inactivated fetal bovine serum (Gibco, Thermo Scientific, Waltham, Massachusetts, USA) 2 mM L-glutamine (Sigma, St Louis, Missouri, USA) and 10 μl/ml of Penicillin and Streptomycin (Sigma). Cells were seeded (5×10^4/well) on 96 well plates one day before the experiment. Ascending concentration series of CeO_2, CeO_2@$mSiO_2$, and the CeO_2@$mSiO_2$-Cap@Chit NAB and capsaicin solution were added to cells in triplicates and the cell viability was measured by employing the colorimetric WST-1 Cell Proliferation Assay (Roche, Basel, Switzerland). The protocol provided by manufacturer was followed. Briefly, treated cells were incubated 24 h in CO_2 incubator at 37 °C whereafter the WST-1 reagent was added to the cells. The absorbance of the colored formazan was measured at 430 nm after 2 h using a Varioskan microplate reader (Thermo Scientific).

2.5. Antibacterial activity of NAB against E. coli

Ampicillin-resistant *E. coli* was obtained by transforming the *E. coli* Top10 strain (ThermoFisher Scientific) with the plasmid pMT/Flag-His containing an ampicillin resistance gene. Ampicillin-resistant *E. coli* can be distinguished from resident bacteria by culturing in ampicillin-containing media. Fresh cultures of *E. coli* were prepared for each experiment by scooping 2–4 colonies from on Luria-Bertani (LB) (Sigma) agar plate, dispersing them in LB broth containing 0.1 mg/ml Ampicillin (Sigma) and incubating overnight in a shaker at 37 °C, 180 rpm. From this overnight grown pre-culture, 10^5 CFU/ml of the test bacteria strain were cultured. The cultures were treated with NAB, CeO_2, CeO_2@$mSiO_2$ or CeO_2@$mSiO_2$-Cap@Chit, all at a final concentration of 10 μg/ml, 50 μg/ml, 100 μg/ml, or 200 μg/ml, except forCeO_2 NP, which was investigated at concentrations of 1 μg/ml, 5 μg/ml, 10 μg/ml and 20 μg/ml. The concentrations are estimates based on the CeO_2 content in CeO_2@$mSiO_2$ samples from ICP-MS measurements (data not presented).

Optical density (OD) measurements during the treatment of the bacterial cultures and counting of colony forming units (CFU) after nanocomposite treatments were performed. In the first method, OD_{600} values were monitored for 24 h with the Bioscreen C MBR (Oy Growth Curves Ab Ltd., Finland) multiplate reader. Based on the obtained OD_{600} values the growth profile of bacteria was plotted. The exponential phase of the growth profiles was identified, and the impact of CeO_2, CeO_2@$mSiO_2$ CeO_2@$mSiO_2$@Chit and NAB treatment on the doubling time of the bacteria were calculated. Growth inhibition percentage *vs* time graphs were plotted in order to identify the impact of the employed treatments during the exponential phase of the bacterial growth.

The short-term antibacterial effect was investigated by employing colony counting assay in order to clarify whether the recovery of NAB and its construction units treated bacteria was possible before their exponential growth phase had started and adapt the treatment conditions. For this purpose, cultured bacteria were adjusted to 10^5 CFU/ml, added to 24 well plates, and supplemented with the nanocomposites at concentrations given in the previous method at 37 °C for 4 h. 4 hours incubation time point was chosen based on the obtained growth profile curves, as the closest time point prior to exponential phase of the treated bacteria growth curve. The untreated bacteria culture was used as a negative control. 30 μl treated bacteria culture was plated on LB-agar plates and the plates were incubated at 37 °C for 24 h, whereafter the colonies were counted.

2.6. Effect of NAB on the morphology of the bacteria

The morphology of treated bacteria was investigated with Scanning Electron Microscope (FEI Quanta-200 MK2) with an accelerating voltage of 20 kV. The bacteria were treated with the concentrations of NAB and its constructs as specified in Section 2.4. Untreated bacteria were used as negative controls. After 4 h incubation, cultures were centrifuged at 6000 rpm. The pellet was washed thrice with phosphate buffer saline (PBS) and was finally diluted 100 times with PBS. A drop of the diluted samples was added onto a 1cm x 1cm glass plate and air-dried. The samples were fixed with 2.5% glutaraldehyde for 30 min. The samples were further washed with water three times and then gradually dehydrated with ethanol at room temperature and imaged.

2.7. Imaging NAB in intestines of Drosophila larvae

To enable fluorescent detection of NAB, the particle design was modified by replacing the capsaicin in CeO_2@mSiO_2-Cap@Chit with a fluorophore, DiI (1,1′-dioctadecyl-3,3,3′,3′-tetramethindocarbocyanine perchlorate), named here NAB/DiI. *D. melanogaster Canton*^{S} 3rd instar larvae were fed Nutrifly BF™ fly food (Dutscher Scientific) supplemented with 0.3 mg/ml NAB/DiI for two hours at 25 °C. The presence of NAB/DiI in 3rd instar larvae were visualized using a Leica MZ6 stereo microscopy (Wetzlar, Germany). All use of *D. melanogaster* is approved by the Finnish Board for Gene Technology.

2.8. Investigation of bacterial growth in intestines of NAB fed Drosophila larvae

The fruit fly, *D. melanogaster* was used as an *in vivo* model to investigate the use of the designed NAB in combating ingested bacteria. *E. coli* transformed with pMT/Flag-His were cultivated in LB medium at 37 °C for 16–18 h. 3rd instar *Canton*^{S} larvae were orally infected by feeding with transformed *E. coli* diluted in food 1:3, for 5 h at 25 °C and thereafter transferred to bacteria-free food supplemented with 0.3 mg/ml NAB or with ascending concentrations of capsaicin (0.14 mg/ml, 1 mg/ml, 2 mg/ml or 4 mg/ml) for 2 h at 25 °C. The value of 0.14 mg/ml was included as it corresponds to the exact amount of loaded capsaicin in the NAB design. After feeding, the larvae were washed twice in sterile H_2O, homogenized in PBS, and plated on ampicillin-LB-agar plates. Samples were taken from two larvae per triplicate and the number of *E. coli* colonies was counted after 24 h of incubation at 37 °C. *In vivo* growth inhibition by NAB was evaluated by using an unpaired Mann-Whitney test for statistical significance.

3. Results

3.1. Characterization of NAB with constructs and release of capsaicin and cerium ions

To characterize the synthesized NAB and its constructs, we measured hydrodynamic size (DLS), the polydispersity index (PDI), and net surface charge (ζ-potential) of their dispersions. The synthesized CeO_2 NP in suspension yielded a net positive surface charge (ζ-potential) at pH 5 and a hydrodynamic size value above 100 nm with a PDI value of 0.2 (Table 1).

The values from the DLS analysis indicated that the CeO_2 NP were present in the form of aggregates, as the actual CeO_2 NP sizes observed from TEM imaging were determined to be approximately 20–30 nm (Fig. 1a). Mesoporous silica shell (mSiO_2) formation around CeO_2 NP, ceria (Fig. 1b) aided in the lowering of the polydispersity index (PDI) values from 0.2 to 0.1.

Here, the porous shell is employed mainly to function as reservoir for antibacterial compounds to improve the antibacterial action of the resulting composite. However, the antibacterial compounds can be replaced with virtually any other molecular agent *e.g.* fluorescent dyes for imaging; in the circumstance of tracing of the nanocomposite structure in *in vivo* models is required. Clear changes in the hydrodynamic size and net surface charge values were observed after coating with the porous shell (CeO_2@mSiO_2) yielding a higher hydrodynamic size value of approximately 300 nm and a lower absolute ζ-potential compared to the CeO_2 NP core. We note that DLS measurement is suitable for verifying the dispersed state of nanoparticles in solution, rather than as an actual size determination method. After capsaicin loading, successful chitosan coating on CeO_2@mSiO_2-Cap was confirmed by a significant increase in ζ-potential values from −5.11 ± 0.15 mV (for CeO_2@mSiO_2) to +33.3 ± 0.99 mV (for CeO_2@mSiO_2-Cap@Chit), in accordance with our previous studies comprising chitosan coatings [22]. The structural integrity of the nanocomposites is preserved after incorporating all design components, *i.e.* the antibacterial agent capsaicin and the antibacterial polymer chitosan (Fig. 1c and d).The particle size distribution analysis from TEM images (Fig. S2) revealed that more than 70% of particles (out of 1113 analyzed CeO_2@mSiO_2) show spherical morphology with an aspect ratio of 1.0–1.1 and were within the size range of 118–169 nm. When utilizing the porous shell as drug reservoir, we achieved approximately 30 w/w% capsaicin loading, with respect to the full nanocomposite weight, as the highest loading degree prior to chitosan coating (Fig. S1). Leakage of capsaicin during the chitosan coating of CeO_2@mSiO_2-Cap was less than 5% of the loaded capsaicin (w/w% with respect to loaded capsaicin amount). The final amount of capsaicin was calculated as 28.5 w/w% with respect to the total NAB weight. The capsaicin release from CeO_2@mSiO_2-Cap and NAB was followed (Fig. S3) up to 24 h. Differences in drug release profiles was observed in the first 10 h (Fig. 2a). Released drug concentration in pH 7.2 and pH 5 buffer solution was 62.6 ± 5.5 μg/ml and 100.2 ± 4.8 μg/ml, respectively, during the first hours. Under both pH conditions, the obtained values are higher than the solubility limit of capsaicin in water, 28.9 μg/ml [27]. However, no capsaicin precipitation was observed during the experiments. This is most likely due to the NAB formulation enhancing the solubility of the capsaicin; a well-known property of mesoporous silica matrixes [28]. The findings indicated that a higher amount of capsaicin was released from NAB in acetate buffer solution (pH 5) than in HEPES buffer solution (pH 7.2). It is known that chitosan forms a gel-like structure which is insoluble under basic conditions, hence preventing drug release at pH 7.2. When the pH is below isoelectric point (IEP) of chitosan (6.3), the drug is released due to protonation of the amino group on chitosan [29]. Less than 40% relative capsaicin was released in all studied conditions, which could be due to non-sink testing conditions provided with 1 mg/ml NAB contains 340 μg/ml capsaicin in order to prevent the NAB structural dissolution, which may further induce the drug release [30].

Decreasing trend was observed for the cerium elemental release profile of CeO_2@mSiO_2@Chit samples compared to CeO_2@mSiO_2 samples (Fig. 2b) after 8 h. which could be due to the chitosan layer on the core@shell design, as chitosan can adsorb trace metals and induce cerium complexation [15,16].

Table 1
Hydrodynamic size (DLS), their respective polydispersity index (PDI), and net surface charge (ζ-potential) measurements (n ≥ 3) of NAB and its constructs.

Sample	Hydrodynamic size in Milli-Q water (nm)	Polydispersity index (PDI)	ζ-potential (mV) in Acetate buffer (@pH 5, 10 mM)
CeO_2 NP	113.8 ± 2.3	0.2 ± 0.04	+32.7 ± 1.3
CeO_2@mSiO_2	339.9 ± 1.3	0.1 ± 0.1	−5.1 ± 0.1
CeO_2@mSiO_2-Cap	315.1 ± 2.8	0.2 ± 0.0	−8.5 ± 0.6
NAB	943.8 ± 70.9	0.2 ± 0.1	+33.3 ± 0.9

3.2. Evaluation of the mammalian cytocompatibility of NAB and its components

To test whether mammalian cells tolerated NAB and its constructs, their cytotoxicity was addressed on cultured cancerous human epithelial Caco-2 cells. NAB, CeO_2@mSiO_2 and CeO_2 NP were cytocompatible up to 200 μg/ml (Fig. 3a). IC50 values were 347 μg/ml, 700 μg/ml, 228 μg/ml, 37 μg/ml respectively for CeO_2, CeO_2@mSiO_2, NAB and capsaicin (Fig. S4). The obtained results were employed for approximating a safe dosing regime for all the samples and also nanocomposite concentration that will not lead

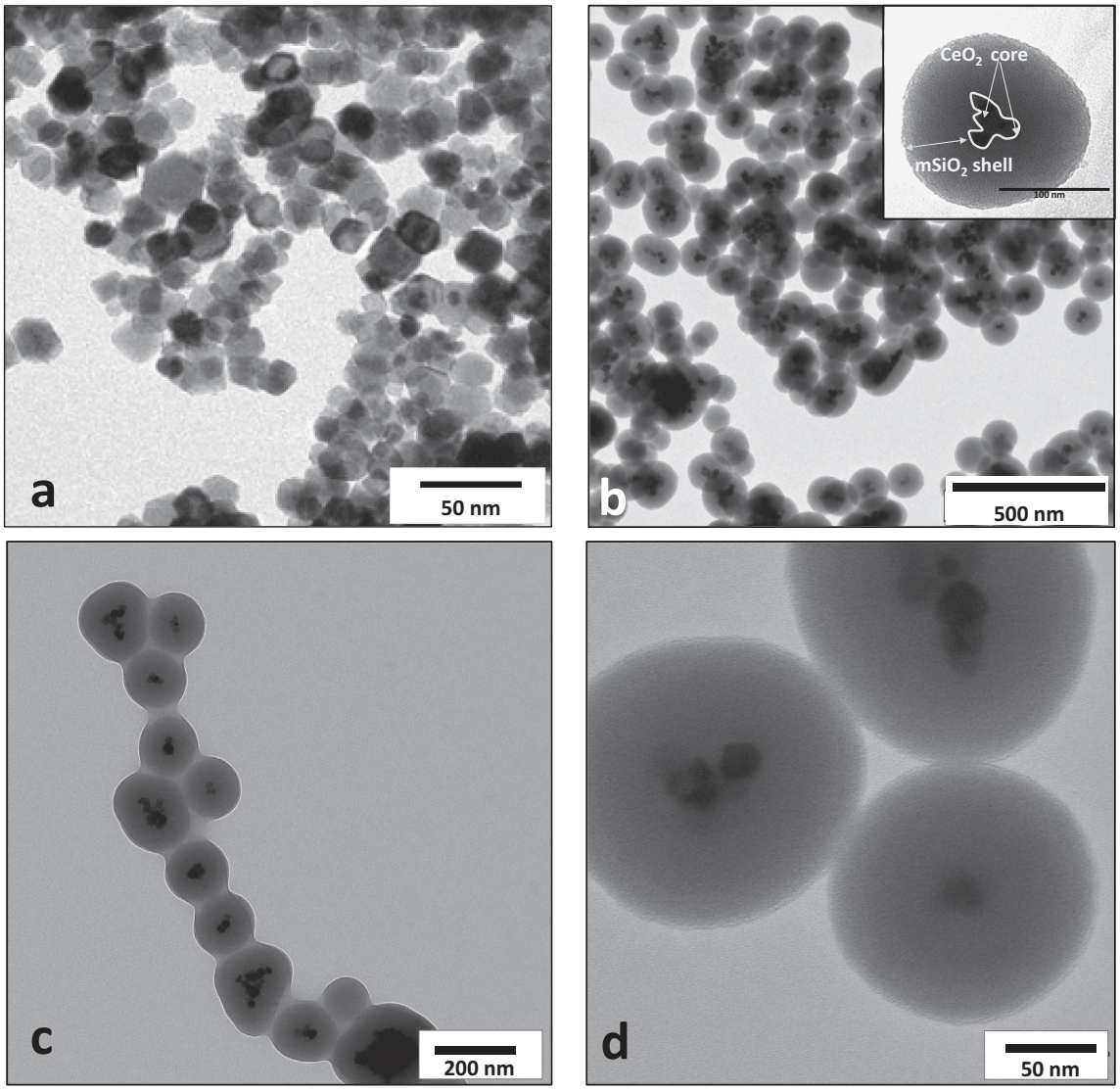

Fig. 1. a) TEM images of CeO_2 NP (b) CeO_2@$mSiO_2$, inset showing the porous shell coating (c) CeO_2@$mSiO_2$-Cap and (d) NAB.

sedimentation during the application. Importantly, incorporation of capsaicin into CeO_2@$mSiO_2$@Chit reduced the cytotoxic effect of capsaicin by providing a reservoir for its delivery. It is also evident that increasing the concentration of free capsaicin leads to decreased cell viability, but free capsaicin was toxic already at 1 μg/ml concentration (Fig. 3b). NAB could thus serve for improving the cytocompatibility of capsaicin against mammalian cells and prevention of irritation in the gastrointestinal tract during oral administration [31] which was also corroborated by the cytotoxicity investigations of free capsaicin equivalent to content in the composite design.

3.2.1. Bacterial growth inhibition by NAB and its constructs

The antibacterial properties of NAB and its constructs were verified by incubating *E. coli* suspensions with the particles followed by optical measurement (OD_{600}) of bacteria suspension. The lowest optical density

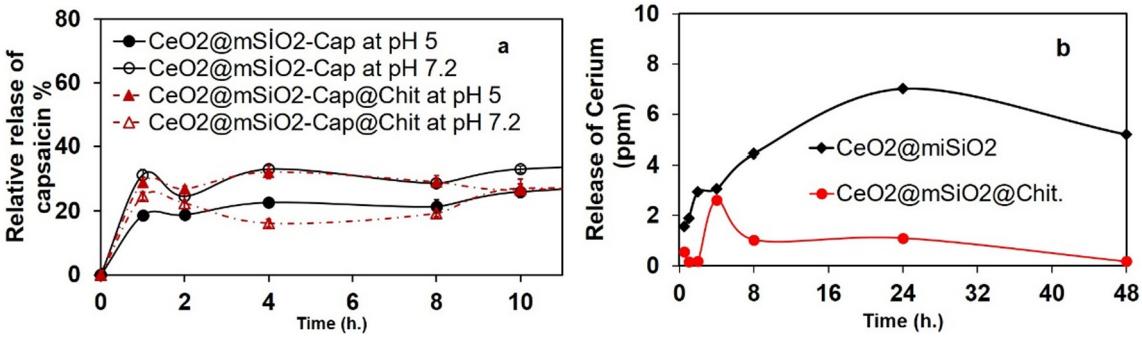

Fig. 2. a) Relative percentage of released capsaicin with respect to the loaded content of capsaicin in CeO_2@$mSiO_2$_Cap and NAB samples at pH: 7.2 and pH 5 for 10 h. b) Cerium release profile from CeO_2@$mSiO_2$ and CeO_2@$mSiO_2$@Chit over time.

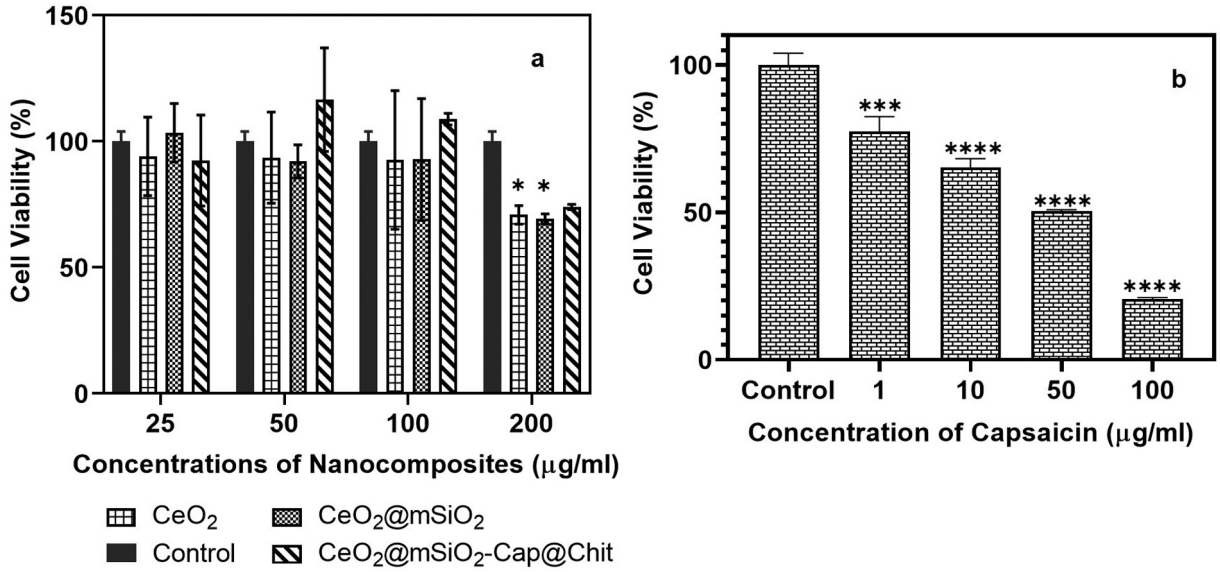

Fig. 3. a) Cytocompatibility of CeO_2, CeO_2@$mSiO_2$, CeO_2@$mSiO_2$-Cap and NAB with Caco-2 cells b) *In vitro* cytocompatibility of capsaicin. Error bars represents SD ($n \geq 3$). The results for both investigation were statistically analyzed with Graphpad Prism software (V 8.4.2) by two-way ANOVA followed by Dunnett's multiple comparisons test. The degree of significance for both graphs were **** $p < 0.0001$, *** $p < 0.0002$, * $p < 0.0332$.

(OD_{600}) values were obtained by NAB and CeO_2@$mSiO_2$@Chit treatment of the bacteria suspension (Fig. 4a). The OD_{600} values of bacterial suspensions treated with NAB and its constructs are presented for ascending concentrations (Fig. S5). We found that the 50 μg/ml dose of CeO_2@$mSiO_2$@Chit and NAB, which was well tolerated by eukaryotic cells, was sufficient to reduce the bacterial growth (Fig. 4a). Interestingly, a change in shape was observed with SEM analysis when comparing NAB treated *E. coli* with untreated bacteria (Fig. 4b and c).

Furthermore, growth profiles in Fig. 4a were employed to plot In (OD_{600}) *vs.* time to identify the growth phases of nanocomposite-treated bacteria [32]. The exponential phase of untreated bacteria culture was depicted to be between 3 h and 7 h. The treatment of bacteria with NAB, CeO_2@$mSiO_2$@Chit, and CeO_2 NP led to shortening of the exponential phase from 4 h to 3 h. However, the treatment of bacteria with CeO_2@$mSiO_2$ composite did not cause a shortening of the exponential phase duration. Specific growth rate of treated bacteria during the exponential phase

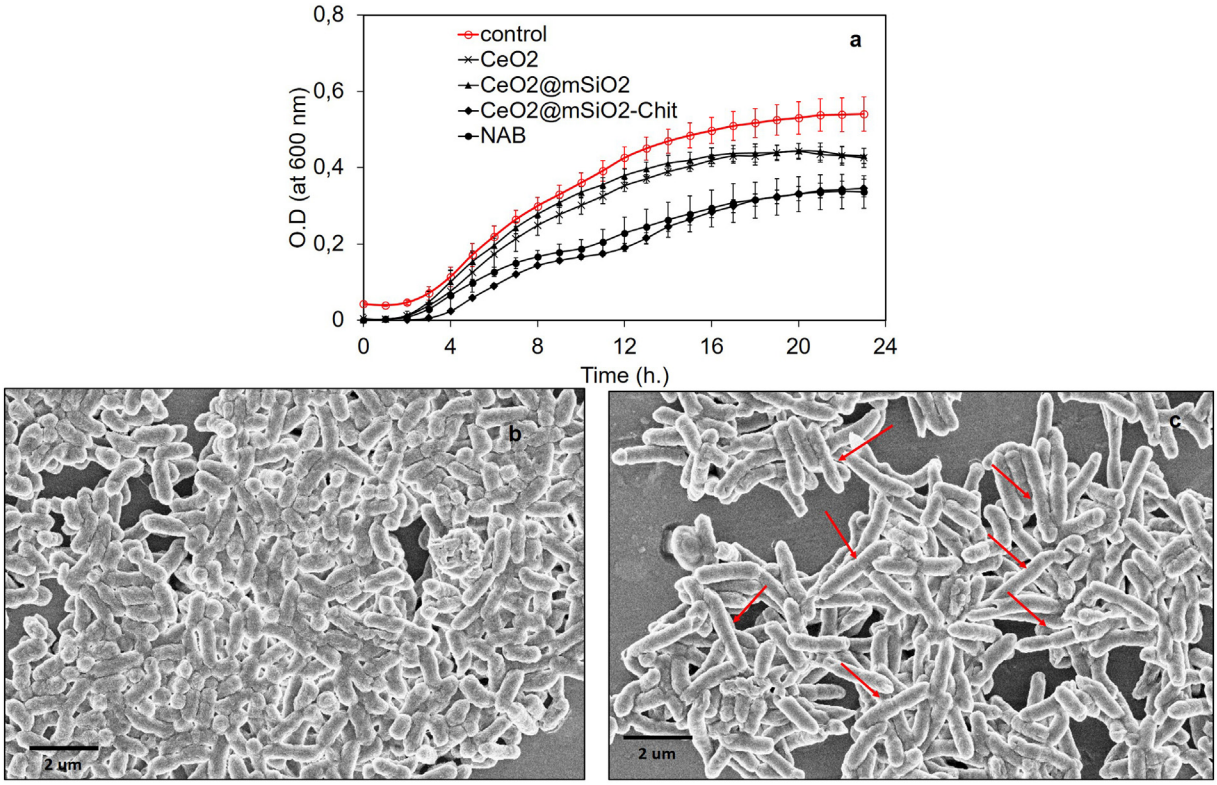

Fig. 4. a) Effect of CeO_2, CeO_2@$mSiO_2$, CeO2@$mSiO_2$@Chit samples, and NAB on the growth kinetics of *E. coli*. The effective dose of CeO_2@$mSiO_2$, CeO_2@$mSiO_2$@Chit, and NAB is 50 μg/ml in all experiments and for CeO_2 the effective dose is 5 μg/ml. b) Scanning electron microscopic images of untreated *E. coli* (Mag. 5kX). c) Scanning electron microscopic images of *E. coli* in the presence of NAB (Mag. 5kX, red arrow points the elongated *E. coli*).

was calculated by employing Eq. (1) [33,34]. OD1 and OD2 correspond to the OD values at the time points at the beginning of the exponential phase (t1) and end of the exponential phase (t2), respectively.

$$\mu = \frac{InOD2 - In\ OD1}{(t2 - t1)} \quad (1)$$

The specific growth rates of bacteria treated with NAB and its construction units were 1.14 h^{-1}, 1.17 h^{-1}, 1.34 h^{-1} and 1.09 h^{-1} for CeO_2, CeO_2@mSiO_2, CeO_2@mSiO2@Chit, and NAB treated bacteria respectively; while untreated bacteria displayed a growth rate of 0.40 h^{-1} during the exponential growth phase of the culture. The obtained OD values for the higher concentration treatments were not employed to calculate the growth inhibition percentage, due to the aggregation potential of nanoparticles in bacterial culture media during the incubation time. This phenomenon may affect the biological activity of nanoparticles and result in misleading data for evaluating the cell and nanoparticles interactions and hence, the obtained antibacterial activity [35,36]. The cultivable status and adapting of bacteria to NAB and its construction units containing incubation media after the 4-h treatment are presented in Fig. 5. The time point 4 h was chosen, as it is the beginning of the exponential phase for NAB treated bacterial cultures, and thus provides an understanding on the impact of stress by NAB presence on the cultivable state of bacteria prior to exponential phase. As shown in Fig. 5, the NAB treatment of bacteria results in complete growth-inhibition after 4 h of incubation.

3.3. In vivo evaluation of the antibacterial activity of NAB

To investigate if NAB can reduce the growth capacity of bacteria *in vivo* in the intestine of *Drosophila melanogaster*, third instar larvae were fed with fluorescent NAB. The ingestion of particles was followed by feeding CeO_2@mSiO_2-Cap@Chit particles in which capsaicin was replaced with the fluorophore DiI (NAB/DiI). The ingested NAB/DiI was clearly visible in the intestine of *Drosophila* larvae after a 2-h treatment (Fig. 6a).

To test the antibacterial activity of NAB *in vivo*, *E. coli* growth was determined in orally infected third instar *Drosophila* larvae treated with food supplemented with NAB or different concentrations of free capsaicin after infection. While a concentration of 0.3 mg NAB/ml was enough to inhibit bacterial growth in the *Drosophila* intestine (Fig. 6b), free capsaicin concentrations of 1 mg/ml and higher were required to decrease the amount of *E. coli* (Fig. 6c). The lowest concentration of free capsaicin, 0.14 mg/ml, corresponds to the loaded degree of capsaicin in NAB.

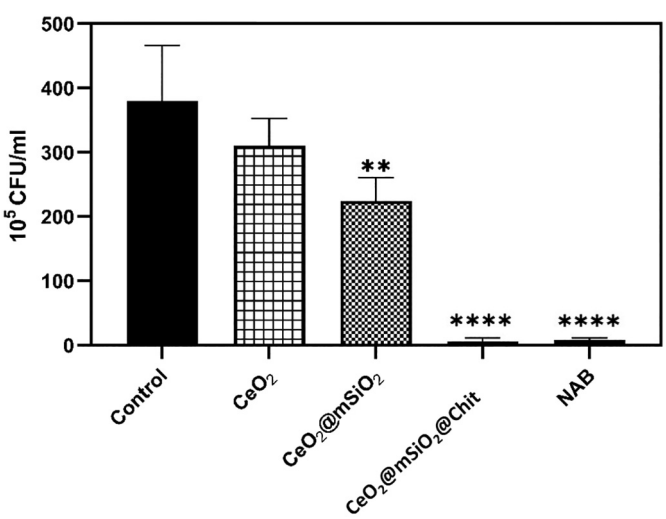

Fig. 5. Recovered viable number of *E. coli* colonies (CFU/ml) after 4 h of treatment with NAB and its construction units. For the analysis, ordinary one-way ANOVA followed by Dunnett's multiple comparisons test was performed and level of significance values were set as **$p < 0.01$ and ****$p < 0.0001$.

4. Discussion

Metal and metal oxide nanoparticles have been employed as antibacterial agents for several decades [37]. However, the antibacterial effect and the cytocompatibility of the particles have been restricted partly due to the problem of their dispersibility in suspension form. Among the employed metal oxide nanoparticles, CeO_2 NP has attracted great interest in antibacterial applications [5]. In various studies, researchers have investigated the size-dependent antibacterial activity of cerium oxide. However, the results have been contradictory and some studies have even concluded insignificant antibacterial effect once the CeO_2 is lowered to nano-scale [38]. CeO_2 NP has a tendency to aggregate under aqueous conditions due to their high surface-to-volume ratio and lack of inherent colloidal stabilization mechanism. This aggregation-tendency of nanoparticles hampers their applicability prospects. The dispersibility of CeO_2 is affected by several factors, among these temperature, surface atomic arrangements, inorganic or organic ligands adsorbed on its surface, ions in solution and their levels, and pH [39]. Further, any additional physically adsorbed layers on ceria surfaces are known to block the NP's reactive surface sites and could inhibit the redox properties, which is depicted as a destructive effect for the colloidal stability of CeO_2 NP [40]. However, the covalent conjugation or shell type coatings are thought not to cause any changes on the surface sites of the CeO_2 NP [39]. The presented surface modification with a mesoporous silica shell may improve the dispersibility of CeO_2 NP in addition to acting as a scaffold for introducing molecular antibacterial agents to redound antibacterial activity. Nevertheless, even though the colloidal stability of CeO_2 NP could be improved by the porous silica shell coating, it has resulted in net negative surface charge values that could inhibit the interaction of nanoparticles with the bacterial cell wall [41].

Designing antibacterial nanoparticles with a positive surface charge to improve the interaction of particles with the negatively charged bacterial cell wall has been proven efficient [41]. Therefore, the net surface charge of the CeO_2@mSiO_2 particulates was modified by employing a cationic polymer, chitosan, which eliminate the negative impact of bare mesoporous silica, while also exploiting the antibacterial properties of chitosan [42]. This improves the interaction between the nanocomposites and Gram-negative bacteria that are covered by peptidoglycans, phospholipids and lipopolysaccharides with a strongly negative charge [43,44]. In addition to the cationic surface properties provided by chitosan, the presence of this coating may also serve to chelate the dissolved cerium ions from the nanocomposite core and increase the solubility of capsaicin, which could improve the overall antibacterial activity of the CeO_2@mSiO_2. Similarly, formation of cerium ion complexes with the functional groups of chitosan macromolecules has been observed to lead to a prolonged-release on demand [45]. Furthermore, studies on antibacterial polymeric scaffolds made by embedding cerium ion-doped fluorapatite into chitosan revealed that doping with Ce^{3+} retains the good antibacterial profile of fluorapatite, suggesting an option for dealing with conditions where tissue healing is compromised by bacterial contamination. Incorporation of capsaicin into nanoformulations to reduce cytotoxicity and pungency, and to improve solubility in aqueous physiological environments could be achieved. It has been shown that encapsulation of capsaicin into chitosan nanoparticles can reduce or even abolish their cytotoxic effect [46–48]. The present chitosan coating in the NAB design could also serve for improving the cytocompatibility of CeO_2@mSiO_2-Cap, as shown in Fig. 3a. The investigations regarding eradication of *E. coli* by free capsaicin *vs.* NAB- in the fruit fly showed that NAB, in addition of consisting of several antibacterial components, could indeed serve as antibacterial drug carrier. We and others have revealed that the mesoporous silica matrix is a vehicle that can merge the benefits of combinatory treatment therapy and nanoparticle-based delivery [49,50].

In our findings, NAB treatment leads to increment in the specific growth rate during the exponential phase and changes in the bacterial shape. It is known that bacterial length can be altered *via* nutrients that affect the regulation of the division machinery. An increased doubling time results in growing into elongated structures that are no longer viable [51,52].

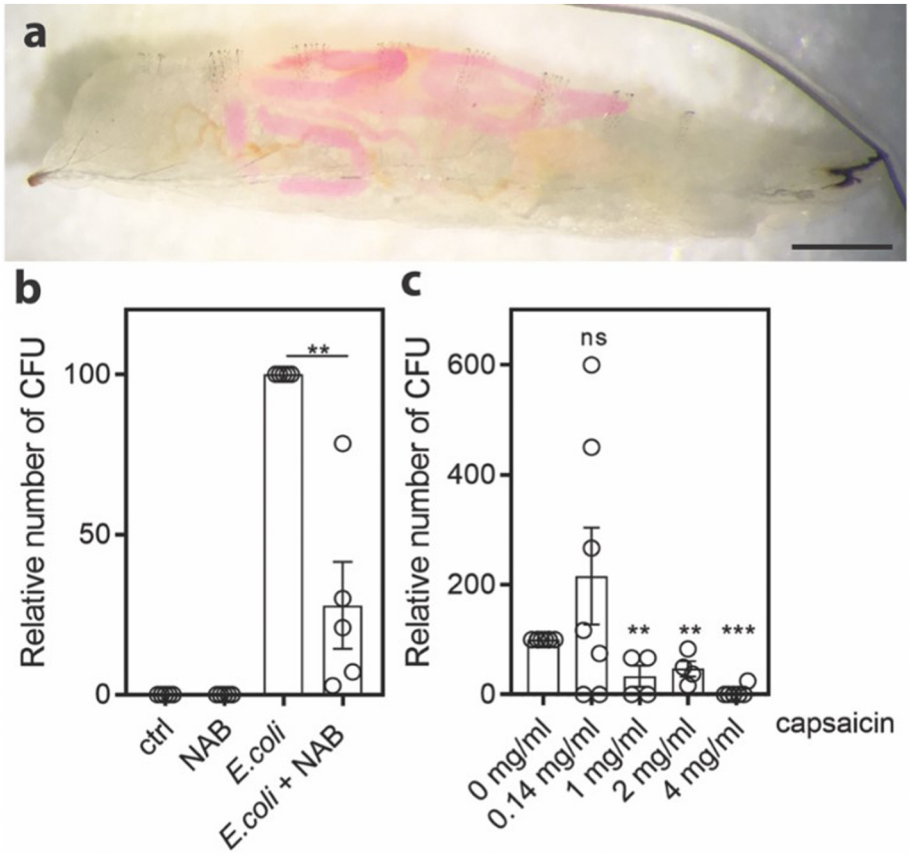

Fig. 6. a) *Drosophila* larvae fed with NAB/DiI-supplemented food for 2 h at 25 °C were visualized with stereo microscopy, scale bar indicates 0.5 mm. b, c) The mean number of CFU of triplicates was counted in homogenates made of third instar *Canton*^{S} larvae infected orally with Ampicillin-resistant *E. coli* for 5 h, followed by a 2-h treatment with fly food supplemented with (b) 0.3 mg/ml NAB dispersed in acetate buffer or (c) with increasing concentrations of capsaicin. Error bars indicate ± SEM of at least four independent experimental repeats. ns = non-significant, **$p < 0.01$ and ***$p < 0.001$.

E. coli has also been shown to increase in size when grown in carbon-rich conditions [53]. Hence, our observed elongation in *E. coli* may be related to the chitosan coating in NAB design, which provided a carbon-rich nutritious environment during the incubation [54]. A similar bacterial elongation has also been observed when *E.coli* was treated with chitosan-coated mesoporous silica nanoparticles in our previous study [22]. Similarly as others, we found the porous silica shell coating in the design of CeO_2@$mSiO_2$ not to impart any significant antibacterial effect [55]. However, CeO_2@$mSiO_2$@Chit and NAB showed similar degrees of antibacterial activity *in vitro*. In any case, we demonstrate that the mesoporous silica shell can serve as a scaffold for the further functionalization of the nanocomposites and loaded with additional antibacterial compounds, *i.e.* capsaicin and chitosan. Loading of the molecular antibacterial agent into the pores of the silica shell, as well as encapsulating the CeO_2 core also served to improve the cytocompatibility of pure CeO_2 NP as well as that of free capsaicin.

Drosophila serves as an attractive model when assessing the efficiency and potential toxicity of nanoparticles *in vivo* [56]. Furthermore, the high degree of conservation of intestinal structure and function has made the fly a popular model when studying intestinal health and disease progression [57]. Here, we have used *Drosophila* 3rd instar larvae as an *in vivo* model to assess the antimicrobial action of NAB against ingested pathogenic bacteria. The results from our *in vivo* experiments are encouraging in regard of using nanoparticles for targeting pathogenic bacteria residing in the gut. Taken together, we show that the antimicrobial activity of capsaicin can be enhanced *in vivo* in a combinatorial NAB design. The core@shell structured nanocomposite design provides an opportunity to enhance the antibacterial activity of nanoceria by combining different antibacterial components, simultaneously improving the cytocompatibility of the design components.

5. Conclusion

The successful development of a CeO_2@$mSiO_2$-Cap@Chit nanocomposite, denoted NAB, proves both the efficiency and the flexibility of a composite core@shell structure with multiple antibacterial components for combinatorial antibacterial action. 50 μg/ml dose of NAB was sufficient to inhibit the bacterial growth of *E. coli in vitro* and recovery of the bacterial cells after a 4-h treatment. The *in vitro* growth inhibition studies suggested significant antibacterial activity of the full NAB design compared to core only and CeO_2@$mSiO_2$. However, a significant difference in the degree of antibacterial activity was not in this case observed between NAB and CeO_2@$mSiO_2$@Chit; nevertheless, it was important to determine that loading of drugs into the pores of the mesoporous silica shell could be achieved, which would be the primary reason for growing a porous shell. NAB and its construction units could be tolerated at high concentrations of up to 100 μg/ml and aid to eliminate the cytotoxic effect of capsaicin antibacterial agent against mammalian Caco-2 cells by the provided chitosan layer in the NAB design. The *in vivo* studies showed that the developed NAB can be localized to the *Drosophila* gut by oral administration, where it is able to decrease the amount of pathogenic bacteria after a 2-h NAB feeding. The investigations regarding free capsaicin *vs.* NAB-aided eradication of *E. coli* in the fruit fly indicated that NAB, as the full design, could indeed serve as antibacterial drug carrier, in addition to consisting of several antibacterial components. Taken together, we have, by using ceria nanoparticles as core with tunable mesoporous silica as shell, antimicrobial capsaicin as loaded drug, and antibacterial chitosan as final coat, constructed a combinatorial nanoparticle with strong antibacterial properties, functioning both *in vitro* and *in vivo* in the model organism *Drosophila*.

CRediT authorship contribution statement

Conceptualization: Didem Şen Karaman, Annika Meinander, Jessica M. Rosenholm

Ideas; formulation or evolution of overarching research goals and aims

Methodology: Didem Şen Karaman, Annika Meinander,

Development or design of methodology; creation of models

Validation: Prakirth Govardhanam, Alexandra Manea, Christa Kietz, Anna Slita

Verification, whether as a part of the activity or separate, of the overall replication/reproducibility of results/experiments and other research outputs

Formal analysis: Didem Şen Karaman, Christa Kietz, Ayşenur Pamukçu, Prakirth Govardhanam

Application of statistical, mathematical, computational, or other formal techniques to analyze or synthesize study data

Investigation: Didem Şen Karaman, Christa Kietz, Prakirth Govardhanam, Alexandra Manea, Anna Slita, Ayşenur Pamukçu (during the revision process)

Conducting a research and investigation process, specifically performing the experiments, or data/evidence collection

Resources: Annika Meinander, Jessica M. Rosenholm

Provision of study materials, reagents, materials, patients, laboratory samples, animals, instrumentation, computing resources, or other analysis tools

Data Curation: N/A

Management activities to annotate (produce metadata), scrub data and maintain research data (including software code, where it is necessary for interpreting the data itself) for initial use and later reuse

Writing - Original Draft: Didem Şen Karaman, Christa Kietz, Prakirth Govardhanam, Ayşenur Pamukçu.

Preparation, creation and/or presentation of the published work, specifically writing the initial draft (including substantive translation)

Writing - Review & Editing: Didem Şen Karaman, Christa Kietz, Annika Meinander, Jessica M. Rosenholm

Preparation, creation and/or presentation of the published work by those from the original research group, specifically critical review, commentary or revision – including pre-or postpublication stages

Visualization: Didem Şen Karaman, Christa Kietz, Ayşenur Pamukçu

Preparation, creation and/or presentation of the published work, specifically visualization/data presentation.

Supervision: Didem Şen Karaman, Annika Meinander, Jessica M. Rosenholm

Oversight and leadership responsibility for the research activity planning and execution, including mentorship external to the core team.

Declaration of competing interest

The authors declare that they have no known competing financial interests or personal relationships that could have appeared to influence the work reported in this paper.

Acknowledgements

The Academy of Finland (projects #283524, #309374), Doctoral Education Network in Materials Research at Åbo Akademi University, and the Magnus Ehrnrooth and Sigrid Jusélius Foundations (Finland) as well as Medicinska Understödsföreningen Liv & Hälsa (Finland), The Scientific and Technological Research Council of Turkey (project #319S024) are acknowledged for funding support. Transmission electron microscopy (JEM-1400 Plus) imaging facility was provided by the Laboratory of Electron Microscopy, University of Turku, Finland. Diti Desai is acknowledged for guiding in *in vitro* cytotoxicity investigations. Josef Gullmets and Fanny Sundqvist are acknowledged for technical assistance with the *in vivo* experiments. This research was also supported by the Center of Excellence in Cellular Mechanostasis at Åbo Akademi University and the InFLAMES Flagship Programme of the Academy of Finland (# 337530).

Appendix A. Supplementary data

Supplementary data to this article can be found online at https://doi.org/10.1016/j.msec.2021.112607.

References

[1] P.V. Baptista, M.P. McCusker, A. Carvalho, D.A. Ferreira, N.M. Mohan, M. Martins, A.R. Fernandes, Nano-strategies to fight multidrug resistant bacteria—"A battle of the titans", Front. Microbiol. 9 (2018)https://doi.org/10.3389/fmicb.2018.01441.

[2] C. Sahlgren, A. Meinander, H. Zhang, F. Cheng, M. Preis, C. Xu, T.A. Salminen, D. Toivola, D. Abankwa, A. Rosling, D.Ş. Karaman, O.M.H. Salo-Ahen, R. Österbacka, J.E. Eriksson, S. Willför, I. Petre, J. Peltonen, R. Leino, M. Johnson, J. Rosenholm, N. Sandler, Tailored approaches in drug development and diagnostics: from molecular design to biological model systems, Adv. Healthc. Mater. 6 (2017) 1700258, https://doi.org/10.1002/adhm.201700258.

[3] H. Hemeg, Nanomaterials for alternative antibacterial therapy, Int. J. Nanomedicine 12 (2017) 8211–8225, https://doi.org/10.2147/IJN.S132163.

[4] E. Sánchez-López, D. Gomes, G. Esteruelas, L. Bonilla, A.L. Lopez-Machado, R. Galindo, A. Cano, M. Espina, M. Ettcheto, A. Camins, A.M. Silva, A. Durazzo, A. Santini, M.L. Garcia, E.B. Souto, Metal-based nanoparticles as antimicrobial agents: an overview, Nanomaterials 10 (2020) 292, https://doi.org/10.3390/nano10020292.

[5] M. Qi, W. Li, X. Zheng, X. Li, Y. Sun, Y. Wang, C. Li, L. Wang, Cerium and its oxidant-based nanomaterials for antibacterial applications: a state-of-the-art review, Front. Mater. 7 (2020)https://doi.org/10.3389/fmats.2020.00213.

[6] S.C. Gad, Cerium, Encycl. Toxicol, Elsevier 2005, pp. 502–503, https://doi.org/10.1016/B0-12-369400-0/00200-3.

[7] K.R. Singh, V. Nayak, T. Sarkar, R.P. Singh, Cerium oxide nanoparticles: properties, biosynthesis and biomedical application, RSC Adv. 10 (2020) 27194–27214, https://doi.org/10.1039/D0RA04736H.

[8] I.A.P. Farias, C.C.L. dos Santos, F.C. Sampaio, Antimicrobial activity of cerium oxide nanoparticles on opportunistic microorganisms: a systematic review, Biomed. Res. Int. 2018 (2018) 1–14, https://doi.org/10.1155/2018/1923606.

[9] L. Kvítek, A. Panáček, J. Soukupová, M. Kolář, R. Večeřová, R. Prucek, M. Holecová, R. Zbořil, Effect of surfactants and polymers on stability and antibacterial activity of silver nanoparticles (NPs), J. Phys. Chem. C 112 (2008) 5825–5834, https://doi.org/10.1021/jp711616v.

[10] C. Bankier, R.K. Matharu, Y.K. Cheong, G.G. Ren, E. Cloutman-Green, L. Ciric, Synergistic antibacterial effects of metallic nanoparticle combinations, Sci. Rep. 9 (2019)https://doi.org/10.1038/s41598-019-52473-2.

[11] K.S. Kumar, V.B. Kumar, P. Paik, Recent advancement in functional core-shell nanoparticles of polymers: synthesis, physical properties, and applications in medical biotechnology, J. Nanopart. 2013 (2013) 1–24, https://doi.org/10.1155/2013/672059.

[12] K.W. Shah, Nanosynthesis techniques of silica-coated nanostructures, in: G.Z. Kyzas, A.C. Mitropoulos (Eds.), Nov. Nanomater. - Synth. Appl, InTech, 2018https://doi.org/10.5772/intechopen.74097.

[13] M. Zhang, C. Zhang, X. Zhai, F. Luo, Y. Du, C. Yan, Antibacterial mechanism and activity of cerium oxide nanoparticles, Sci. China Mater. 62 (2019) 1727–1739, https://doi.org/10.1007/s40843-019-9471-7.

[14] D. Kar, S. Bandyopadhyay, U. Dimri, D.B. Mondal, P.K. Nanda, A.K. Das, S. Batabyal, P. Dandapat, S. Bandyopadhyay, Antibacterial effect of silver nanoparticles and capsaicin against MDR-ESBL producing Escherichia coli: an in vitro study, Asian Pac. J. Trop. Dis. 6 (2016) 807–810, https://doi.org/10.1016/S2222-1808(16)61135-0.

[15] X. Wang, Y. Du, L. Fan, H. Liu, Y. Hu, Chitosan- metal complexes as antimicrobial agent: synthesis, characterization and structure-activity study, Polym. Bull. 55 (2005) 105–113, https://doi.org/10.1007/s00289-005-0414-1.

[16] H. Kaygusuz, E. Torlak, G. Akın-Evingür, İ. Özen, R. von Klitzing, F.B. Erim, Antimicrobial cerium ion-chitosan crosslinked alginate biopolymer films: a novel and potential wound dressing, Int. J. Biol. Macromol. 105 (2017) 1161–1165, https://doi.org/10.1016/j.ijbiomac.2017.07.144.

[17] D. Raafat, H.-G. Sahl, Chitosan and its antimicrobial potential - a critical literature survey: chitosan and its antimicrobial potential, Microb. Biotechnol. 2 (2009) 186–201, https://doi.org/10.1111/j.1751-7915.2008.00080.x.

[18] R.P. Senthilkumar, V. Bhuvaneshwari, R. Ranjithkumar, S. Sathiyavimal, V. Malayaman, B. Chandarshekar, Synthesis, characterization and antibacterial activity of hybrid chitosan-cerium oxide nanoparticles: as a bionanomaterials, Int. J. Biol. Macromol. 104 (2017) 1746–1752, https://doi.org/10.1016/j.ijbiomac.2017.03.139.

[19] H.-I. Chen, H.-Y. Chang, Synthesis and characterization of nanocrystalline cerium oxide powders by two-stage non-isothermal precipitation, Solid State Commun. 133 (2005) 593–598, https://doi.org/10.1016/j.ssc.2004.12.020.

[20] E. von Haartman, H. Jiang, A.A. Khomich, J. Zhang, S.A. Burikov, T.A. Dolenko, J. Ruokolainen, H. Gu, O.A. Shenderova, I.I. Vlasov, J.M. Rosenholm, Core–shell designs of photoluminescent nanodiamonds with porous silica coatings for bioimaging and drug delivery I: fabrication, J. Mater. Chem. B 1 (2013) 2358, https://doi.org/10.1039/c3tb20308e.

[21] J.M. Rosenholm, E. Peuhu, J.E. Eriksson, C. Sahlgren, M. Lindén, Targeted intracellular delivery of hydrophobic agents using mesoporous hybrid silica nanoparticles as carrier systems, Nano Lett. 9 (2009) 3308–3311, https://doi.org/10.1021/nl901589y.

[22] D. Şen Karaman, S. Sarwar, D. Desai, E.M. Björk, M. Odén, P. Chakrabarti, J.M. Rosenholm, S. Chakraborti, Shape engineering boosts antibacterial activity of chitosan coated mesoporous silica nanoparticle doped with silver: a mechanistic investigation, J. Mater. Chem. B 4 (2016) 3292–3304, https://doi.org/10.1039/C5TB02526E.

[23] C.T. Rueden, J. Schindelin, M.C. Hiner, B.E. DeZonia, A.E. Walter, E.T. Arena, K.W. Eliceiri, Image J2: ImageJ for the next generation of scientific image data, BMC Bioinformatics 18 (2017)https://doi.org/10.1186/s12859-017-1934-z.

[24] M. Kaasalainen, V. Aseyev, E. von Haartman, D.Ş. Karaman, E. Mäkilä, H. Tenhu, J. Rosenholm, J. Salonen, Size, stability, and porosity of mesoporous nanoparticles characterized with light scattering, Nanoscale Res. Lett. 12 (2017)https://doi.org/10.1186/s11671-017-1853-y.
[25] Q. Wang, X. Ma, W. Zhang, H. Pei, Y. Chen, The impact of cerium oxide nanoparticles on tomato (Solanum lycopersicum L.) and its implications for food safety, Metallomics 4 (2012) 1105, https://doi.org/10.1039/c2mt20149f.
[26] E. Fröhlich, Comparison of conventional and advanced in vitro models in the toxicity testing of nanoparticles, Artif. Cells Nanomedicine Biotechnol. 46 (2018) 1091–1107, https://doi.org/10.1080/21691401.2018.1479709.
[27] S. Gv, D.T. Daniel, S. Kv, M. Krk, An alternate solvent for the determination of capsaicin content in chillies by HPLC method, Nat. Prod. Chem. Res. 06 (2018)https://doi.org/10.4172/2329-6836.1000342.
[28] A. Maleki, H. Kettiger, A. Schoubben, J.M. Rosenholm, V. Ambrogi, M. Hamidi, Mesoporous silica materials: from physico-chemical properties to enhanced dissolution of poorly water-soluble drugs, J. Control. Release 262 (2017) 329–347, https://doi.org/10.1016/j.jconrel.2017.07.047.
[29] A. Popat, J. Liu, G.Q.(Max) Lu, S.Z. Qiao, A pH-responsive drug delivery system based on chitosan coated mesoporous silica nanoparticles, J. Mater. Chem. 22 (2012) 11173, https://doi.org/10.1039/c2jm30501a.
[30] E. von Haartman, D. Lindberg, N. Prabhakar, J.M. Rosenholm, On the intracellular release mechanism of hydrophobic cargo and its relation to the biodegradation behavior of mesoporous silica nanocarriers, Eur. J. Pharm. Sci. 95 (2016) 17–27, https://doi.org/10.1016/j.ejps.2016.06.001.
[31] W. Peng, X. Jiang, Y. Zhu, E. Omari-Siaw, W. Deng, J. Yu, X. Xu, W. Zhang, Oral delivery of capsaicin using MPEG-PCL nanoparticles, Acta Pharmacol. Sin. 36 (2015) 139–148, https://doi.org/10.1038/aps.2014.113.
[32] B.G. Hall, H. Acar, A. Nandipati, M. Barlow, Growth rates made easy, Mol. Biol. Evol. 31 (2014) 232–238, https://doi.org/10.1093/molbev/mst187.
[33] F. Widdel, Theory and measurement of bacterial growth, https://www.coursehero.com/file/14195525/Theory-and-Measurement-of-Bacterial-Growth/ 2007.
[34] A.L. McKay, A.C. Peters, J.W.T. Wimpenny, Determining specific growth rates in different regions of salmonella typhimurium colonies, Lett. Appl. Microbiol. 24 (1997) 74–76, https://doi.org/10.1046/j.1472-765X.1997.00354.x.
[35] E.M. Hotze, T. Phenrat, G.V. Lowry, Nanoparticle aggregation: challenges to understanding transport and reactivity in the environment, J. Environ. Qual. 39 (2010) 1909–1924, https://doi.org/10.2134/jeq2009.0462.
[36] E.C. Cho, Q. Zhang, Y. Xia, The effect of sedimentation and diffusion on cellular uptake of gold nanoparticles, Nat. Nanotechnol. 6 (2011) 385–391, https://doi.org/10.1038/nnano.2011.58.
[37] Y.N. Slavin, J. Asnis, U.O. Häfeli, H. Bach, Metal nanoparticles: understanding the mechanisms behind antibacterial activity, J. Nanobiotechnol. 15 (2017)https://doi.org/10.1186/s12951-017-0308-z.
[38] K.V. Hoecke, J.T.K. Quik, J. Mankiewicz-Boczek, K.A.C.D. Schamphelaere, A. Elsaesser, P.V. der Meeren, C. Barnes, G. McKerr, C.V. Howard, D.V.D. Meent, K. Rydzyński, K.A. Dawson, A. Salvati, A. Lesniak, I. Lynch, G. Silversmit, B.D. Samber, L. Vincze, C.R. Janssen, Fate and effects of CeO2 nanoparticles in aquatic ecotoxicity tests, Environ. Sci. Technol. 43 (2009) 4537–4546, https://doi.org/10.1021/es9002444.
[39] E. Grulke, K. Reed, M. Beck, X. Huang, A. Cormack, S. Seal, Nanoceria: factors affecting its pro- and anti-oxidant properties, Environ. Sci. Nano 1 (2014) 429–444, https://doi.org/10.1039/C4EN00105B.
[40] J.R. Ray, X. Wu, C.W. Neil, H. Jung, Z. Li, Y.-S. Jun, Redox chemistry of CeO2 nanoparticles in aquatic systems containing Cr(vi)(aq) and Fe 2+ ions, Environ. Sci. Nano 6 (2019) 2269–2280, https://doi.org/10.1039/C9EN00201D.
[41] A. Abbaszadegan, Y. Ghahramani, A. Gholami, B. Hemmateenejad, S. Dorostkar, M. Nabavizadeh, H. Sharghi, The effect of charge at the surface of silver nanoparticles on antimicrobial activity against gram-positive and gram-negative bacteria: a preliminary study, J. Nanomater. 2015 (2015) 1–8, https://doi.org/10.1155/2015/720654.
[42] J. Li, S. Zhuang, Antibacterial activity of chitosan and its derivatives and their interaction mechanism with bacteria: current state and perspectives, Eur. Polym. J. 138 (2020), 109984https://doi.org/10.1016/j.eurpolymj.2020.109984.
[43] B. Gottenbos, Antimicrobial effects of positively charged surfaces on adhering gram-positive and gram-negative bacteria, J. Antimicrob. Chemother. 48 (2001) 7–13, https://doi.org/10.1093/jac/48.1.7.
[44] L. Qi, Z. Xu, X. Jiang, C. Hu, X. Zou, Preparation and antibacterial activity of chitosan nanoparticles, Carbohydr. Res. 339 (2004) 2693–2700, https://doi.org/10.1016/j.carres.2004.09.007.
[45] M.L. Zheludkevich, J. Tedim, C.S.R. Freire, S.C.M. Fernandes, S. Kallip, A. Lisenkov, A. Gandini, M.G.S. Ferreira, Self-healing protective coatings with "green" chitosan based pre-layer reservoir of corrosion inhibitor, J. Mater. Chem. 21 (2011) 4805, https://doi.org/10.1039/c1jm10304k.
[46] M. Kaiser, S. Pereira, L. Pohl, S. Ketelhut, B. Kemper, C. Gorzelanny, H.-J. Galla, B.M. Moerschbacher, F.M. Goycoolea, Chitosan encapsulation modulates the effect of capsaicin on the tight junctions of MDCK cells, Sci. Rep. 5 (2015)https://doi.org/10.1038/srep10048.
[47] A.Y. Choi, C.-T. Kim, H.Y. Park, H.O. Kim, N.R. Lee, K.E. Lee, H.S. Gwak, Pharmacokinetic characteristics of capsaicin-loaded nanoemulsions fabricated with alginate and chitosan, J. Agric. Food Chem. 61 (2013) 2096–2102, https://doi.org/10.1021/jf3052708.
[48] W.D. Rollyson, C.A. Stover, K.C. Brown, H.E. Perry, C.D. Stevenson, C.A. McNees, J.G. Ball, M.A. Valentovic, P. Dasgupta, Bioavailability of capsaicin and its implications for drug delivery, J. Control. Release 196 (2014) 96–105, https://doi.org/10.1016/j.jconrel.2014.09.027.
[49] J.L. Paris, M. Vallet-Regí, Mesoporous silica nanoparticles for co-delivery of drugs and nucleic acids in oncology: a review, Pharmaceutics 12 (2020) 526, https://doi.org/10.3390/pharmaceutics12060526.
[50] Z. Gounani, M.A. Asadollahi, N. Jannik, J. Pedersen, J.Skov Lyngsø, A. Pedersen, R.L. Meyer Arpanaei, Mesoporous silica nanoparticles carrying multiple antibiotics provide enhanced synergistic effect and improved biocompatibility, Colloids Surf. B: Biointerfaces 175 (2019) 498–508, https://doi.org/10.1016/j.colsurfb.2018.12.035.
[51] S. Cesar, K.C. Huang, Thinking big: the tunability of bacterial cell size, FEMS Microbiol. Rev. 41 (2017) 672–678, https://doi.org/10.1093/femsre/fux026.
[52] J.D. Wang, P.A. Levin, Metabolism, cell growth and the bacterial cell cycle, Nat. Rev. Microbiol. 7 (2009) 822–827, https://doi.org/10.1038/nrmicro2202.
[53] W.D. Donachie, K.J. Begg, Cell length, nucleoid separation, and cell division of rod-shaped and spherical cells of Escherichia coli, J. Bacteriol. 171 (1989) 4633–4639, https://doi.org/10.1128/JB.171.9.4633-4639.1989.
[54] A. Kucinska, R. Golembiewski, J.P. Lukaszewicz, Synthesis of N-rich activated carbons from chitosan by chemical activation, Sci. Adv. Mater. 6 (2014) 290–297, https://doi.org/10.1166/sam.2014.1714.
[55] M. Liong, B. France, K.A. Bradley, J.I. Zink, Antimicrobial activity of silver nanocrystals encapsulated in mesoporous silica nanoparticles, Adv. Mater. 21 (2009) 1684–1689, https://doi.org/10.1002/adma.200802646.
[56] M. Chifiriuc, A. Ratiu, M. Popa, A. Ecovoiu, Drosophotoxicology: an emerging research area for assessing nanoparticles interaction with living organisms, Int. J. Mol. Sci. 17 (2016) 36, https://doi.org/10.3390/ijms17020036.
[57] Y. Apidianakis, L.G. Rahme, Drosophila melanogaster as a model for human intestinal infection and pathology, Dis. Model. Mech. 4 (2011) 21–30, https://doi.org/10.1242/dmm.003970.